THE JOURNAL OF PHYSICAL CHEMISTRY C

Article

Cite This: J. Phys. Chem. C 2019, 123, 10956−10966

pubs.acs.org/JPCC

Influence of Cobalt Crystal Structures on Activation of Nitrogen Molecule: A First-Principles Study

Bing-Yan Zhang,[†,⊥,#] Pei-Pei Chen,[†,⊥,#] Jin-Xun Liu,[*,§] Hai-Yan Su,[‡] and Wei-Xue Li[*,∥]

[†]State Key Laboratory of Catalysis and [‡]State Key Laboratory of Molecular Reaction Dynamics, Dalian Institute of Chemical Physics, Chinese Academy of Sciences, Dalian 116023, China

[§]Department of Chemical Engineering, University of Michigan, Ann Arbor, Michigan 48109-2136, United States

[∥]Department of Chemical Physics, School of Chemistry and Materials Science, University of Science and Technology of China; Hefei National Laboratory for Physical Sciences at the Microscale, Hefei 230026, China

[⊥]University of Chinese Academy of Sciences, Beijing 100049, China

Supporting Information

ABSTRACT: Identification of the structure sensitivity of nitrogen molecule (N_2) activation and ammonia synthesis on metal surfaces is important for the mechanistic understanding and rational design of more efficient catalysts. In the present work, density functional theory calculations together with microkinetic simulations were performed to study the influence of cobalt crystal structures including hexagonal close-packed (HCP) and face-centered cubic (FCC) on nitrogen molecule dissociation and ammonia synthesis. Molecular and dissociative adsorption energies of N_2 as well as dissociation barriers are calculated for a total of ten cobalt surfaces. It is found that molecular adsorption energies on Co surfaces vary modestly on the order of 0.25 eV, whereas dissociative adsorption energies and the corresponding barriers vary considerably in magnitude by about 0.80 eV. First-principles microkinetic simulations show that HCP Co displays higher activity than FCC cobalt for nitrogen molecule dissociation and ammonia synthesis due to the higher intrinsic activity and density of active sites of HCP cobalt. Nitrogen molecule dissociation is the rate-determining step of ammonia synthesis due to the weak interaction between nitrogen and cobalt. The crystal phase sensitivity of nitrogen molecule dissociation on cobalt is compared with the dissociation of an isoelectronic molecule, carbon monoxide on cobalt, ruthenium, and nickel. This work provides valuable insights into nitrogen molecule dissociation and ammonia synthesis on cobalt catalysts with different crystal phases, and highlights the interplay between activated molecules and catalyst composition on the crystal phase sensitivity.

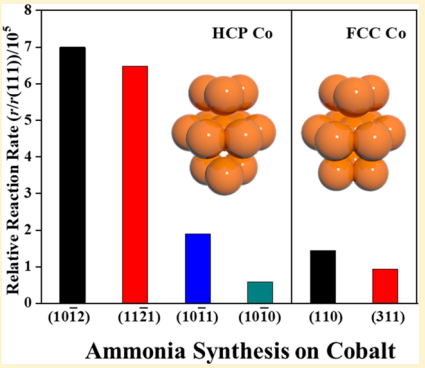

1. INTRODUCTION

The Haber−Bosch process for ammonia synthesis is one of the most significant industrial processes in the last century.[1] The commonly used catalyst for ammonia synthesis is based on iron metal,[2,3] due to its low cost and high activity. Ammonia synthesis requires high temperature and pressure, and further improvements on this energy-intensive process will have an important effect on reducing the consumption of energy resources.[4−6] Thus, numerous investigations have been conducted to find more efficient ammonia synthesis catalysts.[1,7−23] In general, there is a volcano-shaped relationship between nitrogen adsorption energy and the activity of different metal catalysts, with Ru and Os being the best pure metal catalysts for ammonia synthesis.[24] Unfortunately, the high price and the short catalyst lifetime[7] for noble metals hinder their wide industrial-scale applications. Interestingly, although it was previously reported that pristine Co has a lower activity than Fe, Co−Mo alloy material has a higher ammonia synthesis activity than both Fe and Ru catalysts at low NH_3 concentrations.[24] Additionally, a pristine Co-based catalyst promoted by Ba (barium) supported on carbon exhibits greater activity than the commercial Fe-based catalyst for ammonia synthesis.[10] Bulk Re modified with Co has been reported to be particularly active for ammonia synthesis[8] and the catalyst containing BaH_2 and Co sites allows for ammonia synthesis under mild conditions.[22] On the other hand, the produced ammonia only weakly poisons Co-based catalysts unlike Fe-based catalysts, which are strongly poisoned.[10,25] Thus, Co-based catalysts have been regarded as a potential catalyst for ammonia synthesis. Although many works have been conducted on ammonia synthesis based on Co catalysts, how to obtain and optimize even more efficient Co-based catalysts for N_2 activation in ammonia synthesis remains elusive.

The N_2 dissociation step, which is thought as the rate-determining step in ammonia synthesis process,[12,26,27] is

Received: January 20, 2019
Revised: March 27, 2019
Published: April 5, 2019

DOI: 10.1021/acs.jpcc.9b00590
J. Phys. Chem. C 2019, 123, 10956−10966

structure dependent and closely related with surfaces exposed.[28] Heterogeneous catalysts are often very complex solid systems with mixtures of surface active species, a fact of that prevents fundamental understanding of the reaction mechanisms.[29] Thanks to the development of modern surface science technology and density functional theory (DFT) calculations, one can now obtain insights into the atomic-scale properties of solid surfaces with exquisite precision. For instance, the C7 and B5 active sites of Fe-[28] and Ru-based[12,30] catalysts are shown to be critical for the N_2 activation and ammonia synthesis reactions, respectively. To maximize the mass-specific activity, further investigation on the structural sensitivity of ammonia synthesis on Co catalysts is required.

Crystal structure sensitivity has attracted wide attention recently due to the realization that different crystalline phases of the catalysts can lead to distinct catalytic activity and selectivity.[31−51] Co is a commonly used catalysts for Fischer−Tropsch synthesis (FTS) by converting syngas to fuels. Both hexagonal close-packed (HCP) and face-centered cubic (FCC) crystalline phases of Co could coexist under industrial FTS conditions. When decreasing particle size,[52] varying promoter or support, and pretreating the catalysts,[44,53] a transition of the Co crystal phase can occur. In the past few years, experimental investigations have found that HCP Co have higher activity than FCC Co for FTS reactions,[31,35−37,40,43] and FCC Co presents higher methane selectivity.[43] CO activation, which determines the overall FTS reaction activity, is sensitive to the surface structures of catalysts.[54−56] Based on a first-principles kinetic study, we clarified that HCP Co indeed exhibits higher activity than FCC Co for CO activation.[54] The origin of higher activity of HCP Co stems from the high density of favorable active sites on HCP Co that are not available for FCC Co due to their distinct crystal structures and morphologies.[54] In contrast, for Ni and Ru, our recent DFT calculations indicate that metals with the FCC crystal structure are more active than those with HCP crystal structure for CO activation, which mainly stems from exposure of abundant facets with low barrier for CO activation on FCC Ni or FCC Ru.[45,49] Our calculations of the crystal structure effect on CO activation have been confirmed by further experiments and theoretical calculations.[49,57−59]

Many investigations have been performed on Co catalyzing ammonia synthesis. Powder X-ray diffraction (XRD) of unpromoted, reduced, and passivated ammonia synthesis Co samples on active carbon substrates shows that a Co catalyst can coexist in FCC and HCP crystal phases.[11] Additionally, Co deposited on a carbon catalyst was identified as a FCC phase with a little content of HCP Co based on XRD studies performed on the post-NH_3 synthesis Co samples.[25] However, the XRD patterns obtained from slightly passivated, Ba-promoted Co samples using synchrotron radiation reveal that Co can only be detected in its FCC form under NH_3 synthesis conditions.[10] To the best of our knowledge, how the Co crystal structures influence N_2 activation and ammonia synthesis is still an open question. To clarify the structure sensitivity and the active site of Co-based catalysts for ammonia synthesis, we have systematically studied dependence of N_2 activation and ammonia synthesis on Co crystal phases and their associated morphologies in the present work.

Herein, we have performed density functional theory (DFT) calculations to study N_2 activation on all the facets exposed on HCP and FCC Co obtained by Wulff construction.[54] Ammonia synthesis reaction rates are calculated by first-principles microkinetic simulations on HCP Co and FCC Co. The crystal structure sensitivity of N_2 dissociation and ammonia synthesis over Co is investigated, and finally compared with CO dissociation.

2. COMPUTATIONAL DETAILS

Spin-polarized DFT calculations have been performed by using Vienna ab initio simulation package (VASP).[60,61] Projector augmented wave[62] potentials and the generalized gradient approximation with the Perdew−Burke−Ernzerhof exchange−correlation functionals[63] were adopted throughout all the calculations. The plane wave cutoff energy was specified by 400 eV and the convergence threshold for geometry optimizations was set to 1×10^{-4} eV. When all the forces on the atoms are less than 0.02 eV/Å, the geometry optimizations are considered to have been converged. Monkhorst−Pack[64] k-points sampling of $(12 \times 12 \times 8)$ and $(8 \times 8 \times 8)$ were used to obtain accurate bulk HCP Co and FCC Co lattice parameters, respectively. The calculated lattice constants are a = 2.494 Å, c/a = 1.616 for HCP Co and $a = b = c$ = 3.520 Å for FCC Co, which are consistent with previous experiment studies (a = 2.51 Å, c/a = 1.617 for HCP Co[65] and $a = b = c$ = 3.545 Å for FCC Co[35]). The calculated magnetic moments are 1.63 and 1.64 μ/atom for bulk HCP and FCC Co phases, respectively.

Four equivalent HCP (0001) or FCC (111) Co layers slabs separated by a vacuum of 15 Å were used for all the surface calculations, except that five Co layers were used for the FCC (100) surface. A periodic (2×2) unit cell was adopted for all the considered HCP and FCC Co surfaces with the coverage of 1/4. The density of Monkhorst−Pack k-points sampling was kept at ∼0.03 $Å^{-1}$ for all the slabs calculations. Two top equivalent HCP (0001) Co layers of the slabs and the adsorbates were fully relaxed during the geometry optimizations. Further increase of the k-point and cutoff has no influence on the calculated adsorption of nitrogen atom (Table S1). However, increasing the unit cell from (2×2) to (3×3) weakens the binding strength between N and Co, indicating that there is a lateral attraction between dissociated nitrogen atoms on Co surfaces. Kinetic analysis (Figure S3) shows that under the reaction conditions of ammonia synthesis, equilibrium coverage of nitrogen molecules and nitrogen atoms is negligible due to the weak interaction of cobalt toward N_2 molecules and N atoms as found in the context below. The influence of coverage on N_2 adsorption and dissociation is small and therefore neglected here.

The force-reversed method[66] was used to determine the transition states (TSs), and a force tolerance of 0.03 eV/Å was used. Some of the transition states identified were also characterized again by using the climbing-image nudged elastic band method[67] implemented in VASP to reaffirm the identified TSs. Frequency analysis confirmed that all the located TSs have only one imaginary frequency.

The chemisorption or binding energy E_{ads} of the intermediates A (N_2 or N) involved in the N_2 dissociation reaction can be expressed as $E_{ads} = E_{A/slab} - E_{slab} - E_A$, where $E_{A/slab}$ and E_{slab} are the total energies for the slab with chemisorbed species A and the clean surface respectively, and E_A is the radical or molecule A in the gas phase. We selected the N_2 molecule in the gas phase and two separate, most stable adsorbed N atoms as the initial (IS) and final state (FS), respectively. Meanwhile, the N_2 dissociation barrier is calculated as the difference in electronic energy between the transition state (TS) and the IS. Furthermore, the dissociative

DOI: 10.1021/acs.jpcc.9b00590
J. Phys. Chem. C 2019, 123, 10956−10966

adsorption energies of N_2 are the difference between the total energies of the products (FS) and the reactants in the gas phase (IS). The zero-point correction energies are not included in our calculations. The motion of surface atoms at high surface temperature was not considered explicitly in the present work. According to the literature,[6,68] for a single-step unimolecular or bimolecular reaction, the temperature correction for the dissociation barrier is k_bT, about 0.06 eV at 700 K. Compared to the calculated dissociation barriers below, the correction is small and has no influence on understanding the trend of N_2 dissociation between FCC Co and HCP Co.

3. RESULTS

3.1. Morphologies of HCP and FCC Co. HCP Co and FCC Co have different crystal structures and symmetries, which are crucial for the formation of the particle morphologies and the types of exposed facets. The exposed facets of Co are expected to play a significant role in N_2 activation and ammonia synthesis. The morphologies of HCP Co and FCC Co can be approximated by Wulff constructions[69] based on the calculated surface energies. Consequently, the most probable exposed facets and their relative ratios that determine the active site density can be easily acquired. The stacking sequences are quite different for HCP Co and FCC Co, where HCP Co has a stacking sequence of ABABAB..., whereas FCC Co follows a pattern of ABCABC. The FCC Co phase has a higher symmetry than HCP Co, i.e., FCC Co and HCP Co crystalline phases belong to O_h and D_{3h} point group, respectively. The difference in stacking sequence and point group symmetries of HCP Co and FCC Co will give clearly distinct morphologies between them (Figure 1), which

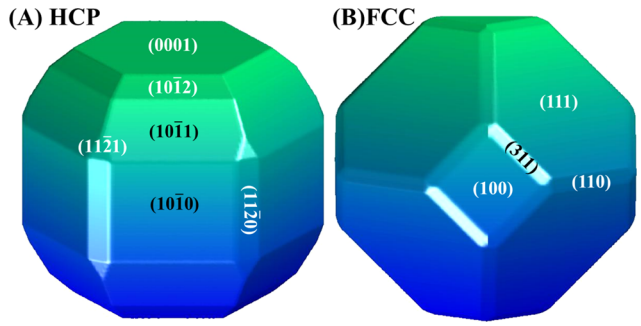

Figure 1. Equilibrium crystal shapes of (A) HCP Co and (B) FCC Co obtained from Wulff construction.[54]

are illustrated extensively in our previous paper.[54] The surface area of the exposed surface in HCP Co and FCC Co morphologies is not only related to the surface energy but also to the orientation of the surface atoms. From our previous calculations, we found that the open corrugated (10$\bar{1}$1) (10$\bar{1}$2), and (11$\bar{2}$1) facets occupy 48% of the total surface area of the HCP Co morphology. In contrast, the close-packed (111) surface has the largest contribution (70%) to the total surface area of FCC Co.

It is worth mentioning that Wulff construction applies mainly for large particle sizes, where the contributions of edge and corner sites are small. We note that the typical particle size of Co particles in ammonia synthesis is 20 nm.[11] This size is relatively large, and the corresponding morphology could be approximated by the above Wulff construction. However, under realistic conditions, the binding strength of reactants and/or intermediates might be sensitive to the surface orientation and coordination of the catalyst. The variation of binding energies could change the corresponding surface energies and even the resulting morphology.[70−73] Nevertheless, as indicated below, due to the weak interaction between nitrogen molecules/nitrogen atoms and Co, the influence of adsorbates on morphology could be modest, in particular, considering the reaction temperature of ammonia synthesis of ∼700 K.

3.2. Adsorption of N_2 and N Atom. We have studied the adsorption of N_2 molecules and N atoms at low coverages (0.25 ML) on all facets exposed on HCP Co and FCC Co Wulff constructions. We explore the adsorption of these intermediates at various high-symmetry sites of each surface. The energetic and geometric information of the most stable adsorption states of N_2 molecules and N atoms on all the considered facets are listed in Table 1, and the corresponding

Table 1. N_2 (E_{N2}) and N (E_N) Adsorption Energies and the Most Stable Dissociative Adsorption Sites of the N Atom on All the HCP and FCC Co Exposed Surfaces[a]

surface	E_{N_2}	E_N	adsorption site	d^N_{N-Co}
			HCP Co	
(10$\bar{1}$1)	−0.60	−6.39	4-fold site	1.861, 1.861, 1.859, 1.859
(10$\bar{1}$0)	−0.58	−5.57	long bridge	1.943, 1.943, 1.811, 1.811
(0001)	−0.46	−5.56	hcp	1.769, 1.769, 1.769
(10$\bar{1}$2)	−0.64	−6.13	4-fold site	1.875, 1.875, 1.882, 1.882
(11$\bar{2}$0)	−0.55	−5.56	hollow	1.965, 1.965, 1.809, 1.875
(11$\bar{2}$1)	−0.67	−5.60	3-fold site	1.772, 1.778, 1.803
			FCC Co	
(111)	−0.42	−5.52	hcp	1.769, 1.769, 1.769
(100)	−0.56	−6.27	4-fold site	1.870, 1.870, 1.870,1.870
(311)	−0.61	−5.79	4-fold site	1.849, 1.849, 1.860, 1.860
(110)	−0.58	−5.57	long-bridge	1.825, 1.825, 1.867, 1.867

[a] d^N_{N-Co} are the nearest distances between N and Co atoms for N adsorption. All adsorption energies are calculated with respect to the corresponding free radical of N atom or N_2 molecule in the gas phase. The energies and distances are in the unit of eV and Å, respectively.

adsorption geometries are also given in Figures 2 and 3. We found that N_2 prefers to bind to one surface Co atom perpendicularly on all the facets exposed on HCP Co and FCC Co Wulff shapes. The calculated N_2 adsorption energies (E_{N_2}) vary from −0.67/(11$\bar{2}$1) to −0.46 eV/(0001) on HCP Co and from −0.61/(311) to −0.42 eV/(111) on FCC Co. N_2 molecules adsorb slightly more weakly on close-packed HCP Co(0001) and FCC Co(111) surfaces than on the corrugated surfaces containing many highly active surface Co atoms with lower coordination number. The overall variation of N_2 adsorption energy is 0.21 eV for HCP Co and 0.19 eV for FCC Co. The simplest standard picture used to describe N_2 chemisorption is an extension of the basic Blyholder model[74,75] for CO−transition metal bonding, which involves σ electron donation from CO to metal orbitals and π back-donation from metal orbitals into $2\pi^*$ orbitals of CO. The weak adsorption of N_2 molecules can be attributed to the weak interaction of the antibonding 2π orbitals with the metal d states.[76] Considering the weak binding between N_2 and Co surfaces, the equilibrium coverages of N_2 on both HCP and FCC Co surfaces will be

DOI: 10.1021/acs.jpcc.9b00590
J. Phys. Chem. C 2019, 123, 10956−10966

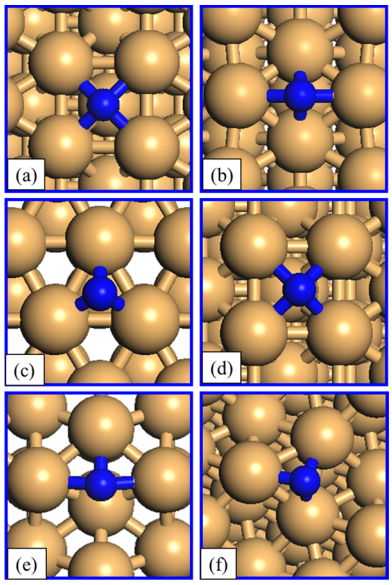

Figure 2. Top view of N atom adsorbed on HCP Co surfaces: (a) $(10\bar{1}1)$; (b) $(10\bar{1}0)$; (c) (0001); (d) $(10\bar{1}2)$; (e) $(11\bar{2}0)$; and (f) $(11\bar{2}1)$. The light orange and blue spheres are Co and N atoms, respectively. This notation is used throughout this paper.

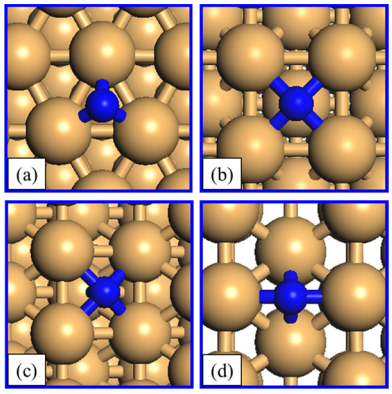

Figure 3. Top view of N atom adsorbed on FCC Co surfaces: (a) (111); (b) (100); (c) (311); and (d) (110).

significantly low under ammonia synthesis conditions of ~700 K.

The binding energies of N atoms can vary in a magnitude of 0.83 eV from −5.56 to −6.39 eV for HCP Co, and spanning 0.75 eV from −5.52 to −6.27 eV for FCC Co. Compared to N_2 adsorption, adsorption of N atoms is structurally more sensitive. Specifically, for HCP Co, N atoms adsorb more stably at the 4-fold site of $(10\bar{1}1)$ and $(10\bar{1}2)$ surfaces with binding energies of −6.39 and −6.13 eV, respectively. However, on the other HCP Co surfaces, N atoms bind weaker at the 3-fold or long bridge sites with similar adsorption energies (−5.56 to −5.60 eV). Similar to HCP Co, N atoms bind stronger at the 4-fold site on (100) and (311) surfaces with the binding energies of −6.27 and −5.79 eV, followed by (111) and (110) surfaces with the binding energies of −5.52 and −5.57 eV at the hcp hollow and long bridge sites, respectively.

As expected, N atoms look for the highest coordination to maximize binding. We note that the lowest binding strength of atomic nitrogen at the four-coordinated site of FCC (311) is −5.79 eV, which is only marginally stronger (0.27 eV at most) than those of two- and three-coordinated sites. However, it is considerably weaker than those on HCP $(10\bar{1}1)$ and FCC (100) with the same four-coordination sites by 0.60 eV and 0.48 eV, respectively. This tells that though the coordination maximization plays a role here, it alone cannot determine the full binding behavior.

3.3. N_2 Activation. In this section, N_2 activation has been studied. The N_2 dissociation barrier, the corresponding reaction energies, and the distances between the two N atoms at TSs on the exposed facets of HCP Co and FCC Co are shown in Table 2. The transition states (TSs) are given in Figures 4 and 5 for HCP Co and FCC Co, respectively. We note that the above calculations show a weak interaction of cobalt toward N_2 molecules and N atoms. This implies that the corresponding coverage under realistic conditions (700 K) would be rather low, as indeed found in the full kinetic analysis (Figure S3). Therefore, the influence of nitrogen coverage on N_2 activation would be modest.

Table 2. Activation Barrier (E_a, eV), Dissociative Adsorption Energies (ΔH, eV) and the Distance between the two N Atoms (d_{N-N}, Å) at Transition State for N_2 Dissociation Reaction on All the HCP and FCC Co Surfaces[a]

HCP Co				FCC Co			
surface	E_a	ΔH	d_{N-N}	surface	E_a	ΔH	d_{N-N}
$(10\bar{1}1)$	0.55	−2.41	1.72	(111)	1.39	−0.65	1.74
$(10\bar{1}0)$	0.70	−0.76	1.79	(100)	1.10	−2.15	1.77
(0001)	1.37	−0.74	1.74	(311)	0.69	−1.19	1.73
$(10\bar{1}2)$	0.54	−1.89	1.94	(110)	0.64	−0.75	1.96
$(11\bar{2}0)$	0.75	−0.75	1.82				
$(11\bar{2}1)$	0.56	−0.82	1.86				

[a]All energies are calculated with respect to N_2 in the gas phase.

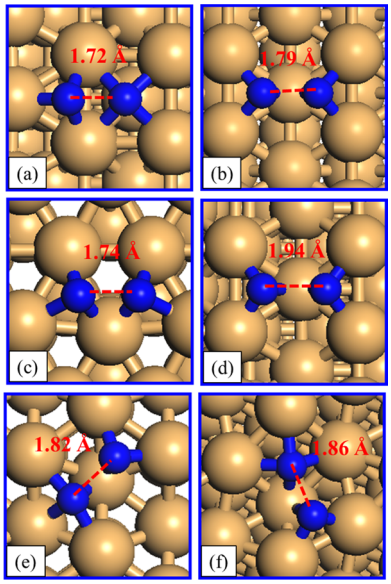

Figure 4. Top view of N_2 dissociation transition-state geometries on HCP Co surfaces: (a) $(10\bar{1}1)$; (b) $(10\bar{1}0)$; (c) (0001); (d) $(10\bar{1}2)$; (e) $(11\bar{2}0)$; and (f) $(11\bar{2}1)$. The bond distance between two N atoms in the transition states are indicated. The light orange and blue spheres are Co and N atoms, respectively. This notation is used throughout this paper.

DOI: 10.1021/acs.jpcc.9b00590
J. Phys. Chem. C 2019, 123, 10956−10966

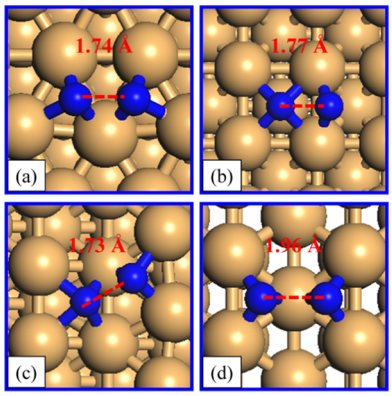

Figure 5. Top view of N_2 dissociation transition-state geometries on FCC Co surfaces: (a) (111); (b) (100); (c) (311); and (d) (110).

Table 2 shows that the reaction energies for N_2 dissociation change significantly with different surfaces. On HCP $(10\bar{1}1)$ and $(10\bar{1}2)$ surfaces, N_2 dissociation is highly exothermic and the corresponding reaction energies are −2.41 and −1.89 eV, respectively. On the other HCP Co surfaces, reaction energies increase up from −0.82 to −0.74 eV. The reaction energies on HCP Co vary largely within a range of 1.67 eV. As for FCC Co, the (100) surface has the highest exothermic reaction energy (ΔH = −2.15 eV), followed by the (311) surface (ΔH = −1.19 eV). The N_2 dissociation is moderately exothermic on the FCC (111) and (110) facets, which have similar reaction energies of −0.65 and −0.75 eV, respectively. The variation of reaction energies is 1.50 eV for FCC Co. Therefore, the HCP $(10\bar{1}1)$, $(10\bar{1}2)$ and FCC (100), (311) surfaces are suggested to be energetically favorable for N_2 dissociation due to their highly exothermic reaction energies for N_2 dissociation on HCP Co and FCC Co, respectively. The large variation of N_2 reaction energies among HCP Co and FCC Co surfaces indicates that N_2 dissociation is strongly sensitive to the crystal structure and surface structure of Co. Moreover, HCP Co is slightly more energetically favorable than FCC Co for N_2 activation because of the presence of HCP $(10\bar{1}1)$ surface possessing a lower exothermic reaction energy as compared with the FCC (100) surface.

N_2 activation barriers were calculated with respect to N_2 in the gas phase (Table 2). Compared to the exothermic adsorption of N_2, the calculated barriers of N_2 dissociation are all positive, indicating a lower dissociation rate as discussed below. Specifically, the N_2 activation barriers on HCP Co facets vary from 0.54 eV on the $(10\bar{1}2)$ to 1.37 eV on the (0001) surface. HCP Co$(10\bar{1}2)$, $(10\bar{1}1)$, and $(11\bar{2}1)$ surfaces have the highest N_2 dissociation activity with similar activation barriers in the region of 0.54−0.56 eV, whereas the HCP $(10\bar{1}0)$ and $(11\bar{2}0)$ surfaces have similar moderate N_2 dissociation barriers of 0.70 and 0.75 eV, respectively. As compared with HCP Co$(10\bar{1}2)$, $(10\bar{1}1)$, and $(11\bar{2}1)$ surfaces, FCC Co(110) and (311) surfaces, which are the most active facets in FCC Co, have lower activity for N_2 dissociation with the activation barrier of 0.64 and 0.69 eV, respectively. The flat HCP Co(0001) and FCC Co(111) and (100) surfaces are least active for N_2 dissociation, with the activation energies as high as almost 1.10 eV. Our calculation results clearly reveal that N_2 dissociation has strong structural sensitive and HCP Co has higher intrinsic activity than FCC Co for N_2 dissociation.

To get an insight into the origin for the high activity of N_2 activation on HCP Co, we carefully analyzed the geometries of N_2 dissociation TSs shown in Figures 4 and 5. First, we compared two representative TS geometries on the HCP $(11\bar{2}1)$ and FCC (311) surfaces with a N_2 activation barrier (E_a) difference of 0.13 eV. These two surfaces are among the most active facets in the corresponding HCP Co and FCC Co shapes with similar TSs. It can be seen that one N atom locates at the 4-fold site stable and alternative N atom moves to the bridge site in N_2 dissociation TSs on these two surfaces. The two N atoms share no Co atoms at the TS on the HCP $(11\bar{2}1)$ facet. This will reduce the repulsive N···N bond interaction originating from bonding competition and Pauli repulsion,[77] stabilizing the corresponding TS compared to that of FCC (311), where two N atoms share one Co atom. Therefore, HCP $(11\bar{2}1)$ is more active than FCC (311). The other two most active HCP $(10\bar{1}2)$ and FCC (110) surfaces also have quite similar TS geometries where two N atoms are bound at a 3-fold site by sharing one Co atom. The N_2 activation barrier on the FCC (110) surface is still 0.1 eV larger than that of the HCP $(10\bar{1}2)$ surface due to the slightly stronger binding strength of N atoms (0.15 eV) during the TS on these two surfaces.

N_2 dissociation on HCP $(10\bar{1}1)$ and FCC (100) surfaces share a similar transition state where one N atom is in a relatively stable 4-fold hollow site, whereas the other N atom moves to a bridge or 3-fold site, respectively. The binding strengths of the N atom at the 4-fold sites (−6.39 and −6.27 eV for HCP $(10\bar{1}1)$ and FCC (100) at the TSs) are strong enough to compensate for the energy cost due to the site competition, thus stabilizing the corresponding TSs geometries and decreasing the N_2 activation barriers (E_a = 0.55 eV for HCP $(10\bar{1}1)$ and E_a = 1.10 eV for FCC (100) surfaces). The largely different N_2 activation barriers between HCP $(10\bar{1}1)$ and FCC (100) surfaces can be ascribed to the N atom binding more strongly at 3-fold sites compared to bridge sites during the TS. Finally, three HCP $(10\bar{1}1)$, $(10\bar{1}2)$, and $(11\bar{2}1)$ surfaces all have lower N_2 activation barriers than the most active FCC (110) surface by almost 0.1 eV. On the other HCP Co$(10\bar{1}0)$, $(11\bar{2}0)$, (0001), and FCC Co(111) surfaces, the two N atoms located at the bridge or 3-fold site share one Co atom in the TSs, which increases the N_2 dissociation barriers. In conclusion, N_2 activation is sensitive to the surface structure and crystal structure of HCP Co and FCC Co, and HCP Co is more active than FCC Co.

3.4. Microkinetic Simulations for Ammonia Synthesis. To shed light on the influence of the crystal structures on ammonia synthesis, we calculated the corresponding reaction rate by assuming N_2 activation as the rate-determining step[78]

$$N_2 + 2^* \rightarrow 2N^* \quad (1)$$

$$N^* + \frac{3}{2}H_2 \leftrightarrow NH_3 + * \quad (2)$$

Equation 1 represents the N_2 dissociative adsorption step. Equation 2 is the hydrogenation of the adsorbed atomic N, and this reaction involves several elementary steps containing the adsorption of H_2 molecules. All NH_x (x = 0−2) hydrogenation steps are in equilibrium, and we do not need to preform DFT calculations for these steps herein. All NH_x hydrogenation steps can thus be merged in the equilibrated reaction step (2).

DOI: 10.1021/acs.jpcc.9b00590
J. Phys. Chem. C 2019, 123, 10956−10966

Therefore, the reaction rate of ammonia synthesis reaction can be given by

$$r = k_1 P_{N_2} \theta_*^2 \left(1 - \frac{P_{NH_3}^2}{K_{eq} P_{N_2} P_{H_2}^3}\right) = k_1 P_{N_2} \theta_*^2 (1 - \gamma) \quad (3)$$

where θ_* stands for the coverage of empty sites. P_{N_2}, P_{H_2}, and P_{NH_3} are the partial pressures of N_2, H_2, and NH_3 gases, respectively. K_{eq} is the equilibrium constant for the ammonia synthesis.

Based on the transition state theory,[79] the reaction rate constant (k_1) for N_2 dissociative adsorption can be given as

$$k_1 = A\, e^{-E_a/k_B T} = \frac{k_B T}{h} \frac{q_{TS}}{q_{N_2}} e^{-E_a/k_B T} \quad (4)$$

Here, A is the prefactor, k_B is the Boltzmann constant, and h is Planck's constant. q_{TS} and q_{N_2} are the partition functions for N_2 in the TS and gas phase (partition functions calculation details are presented in the SI), respectively. The vibration mode leading to the dissociation was excluded in the partition function q_{TS}. Industrial ammonia synthesis conditions (P = 100 bar, T = 700 K, N_2-to-H_2 ratio of 1:3, with 1% NH_3) are considered for ammonia synthesis rate calculations. It was found that partition functions q_{TS} (Table S2) vary slightly from 10 to 19 for HCP Co and from 11 to 19 for FCC Co. Therefore, the value of the prefactor A ($\sim 10^5$), which is proportional to q_{TS}, is also nearly independent of the Co facets and crystal structure. Therefore, N_2 dissociation rate constants (k) closely correlated with N_2 activation energy. The values of k over the most active $(10\bar{1}1)$, $(10\bar{1}2)$, and $(11\bar{2}1)$ surfaces in HCP Co are about more than 4 times larger than that of the most active (110) surface in FCC Co(Table 3).

The relative reaction rates (r) for ammonia synthesis calculated through eq 3 are shown in Table 3 and Figure 6. It is obvious that the three $(10\bar{1}1)$, $(10\bar{1}2)$, and $(11\bar{2}1)$ surfaces in HCP Co display higher ammonia synthesis reaction rates than the most active (110) surface in FCC Co. In spite of this, from Table 3 and Figure 1, we can see that the HCP

Table 3. Surface Area Proportion (S, %),[54] Prefactor (A, s^{-1}), and Reaction Constant (k_1, s^{-1}) for N_2 Dissociative Adsorption Step and the Calculated Reaction Rate for Ammonia Synthesis on HCP Co and FCC Co Surfaces Normalized by that of FCC Co(111) Surface[a]

surface	S[54]	A	k_1	r[b]
		HCP Co		
$(10\bar{1}1)$	35	4.3×10^5	52	1.90×10^5
$(10\bar{1}0)$	28	3.0×10^5	2.9	5.89×10^4
(0001)	18	4.6×10^5	6.9×10^{-5}	1.41
$(10\bar{1}2)$	12	2.5×10^5	35	7.00×10^5
$(11\bar{2}0)$	6	4.4×10^5	1.7	3.46×10^4
$(11\bar{2}1)$	1	3.2×10^5	32	6.48×10^5
		FCC Co		
(111)	70	4.7×10^5	4.9×10^{-5}	1.00
(100)	12	3.3×10^5	4.3×10^{-3}	6.44×10^1
(311)	10	4.1×10^5	4.6	9.35×10^4
(110)	8	2.7×10^5	7.0	1.44×10^5

[a]Industrial ammonia synthesis conditions (P = 100 bar and T = 700 K) were considered in our calculations. [b]All rates are normalized by that of FCC Co(111) surface with units of s^{-1}.

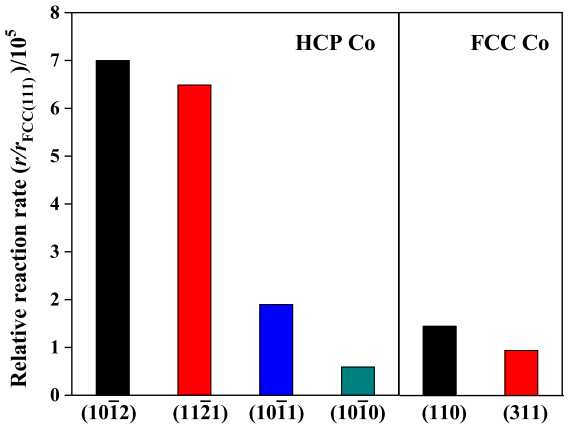

Figure 6. Calculated reaction rate r for ammonia synthesis on highly active HCP Co and FCC Co surfaces at T = 700 K, P = 100 bar conditions. All rates are normalized by that of FCC Co(111) surface with units of s^{-1}.

$(10\bar{1}1)$, $(10\bar{1}2)$, and $(11\bar{2}1)$ surfaces occupy about half of the total surface area of HCP Co morphology, whereas the highly active FCC (110) and (311) surfaces comprise only 18% of the total FCC Wulff construction surface area.[54] As a result, the number of active sites in HCP Co is about 3 times larger than that of FCC Co. HCP Co is more active than FCC Co for N_2 activation and ammonia synthesis due to the higher intrinsic activity and the exposure of greater amount of active sites of HCP Co.

N_2 dissociation as the rate-determining step is valid only when the binding strength of N on metal is weak. In the present work, the binding strength of N on HCP $(10\bar{1}2)$, HCP $(10\bar{1}1)$, and FCC (100) is strong (Table 2), the rate-determining steps could be hydrogenation. As a result, all elementary reaction steps of ammonia synthesis including hydrogenation should be calculated and incorporated in a microkinetic model without assuming any rate-determining step.[80] As an example, we calculated all elementary reaction steps on HCP $(10\bar{1}2)$ and FCC (110) for comparison as well. The calculated potential energy surfaces and the corresponding configurations for ammonia synthesis are shown in Figures 7 and S1, S2, respectively. It can be found that all hydrogenation of NH_x is less structure sensitive to Co surface structures, with the reaction barriers varying from 1.04 to 1.31 eV (Figure 7). Based on these potential energy surfaces, full microkinetics simulations were performed by the MKMCXX package[81−83] without assuming any rate-determining step and equilibration of reactions from NH_x to ammonia (Figure 8). It can be found that the reaction rate of ammonia synthesis on HCP $(10\bar{1}2)$ is about 2−3 times larger than that of FCC (110). Namely, the former is still more active than the latter, and the trend behavior is in good agreement with the above results based on the simplified model. Further kinetic analysis shows that irrespective of the two surfaces considered, the degree of rate control for N_2 dissociation is almost equal to one, meaning that N_2 dissociation is indeed the rat-determining step. This can be rationalized by the low coverage of N_2 and N on Co surfaces due to the weak N_2 adsorption strengths and the high N_2 dissociation barriers (Figure S3).

3.5. Comparison between N_2 and CO on Cobalt.

Isoelectronic N_2 and CO activations are highly structure sensitive. CO activation is a crucial step in the formation of hydrocarbon monomers for FTS. We have found that HCP Co

DOI: 10.1021/acs.jpcc.9b00590
J. Phys. Chem. C 2019, 123, 10956−10966

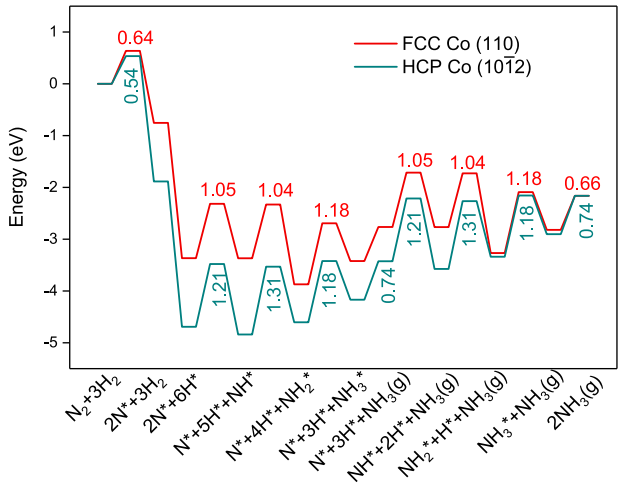

Figure 7. Calculated potential energy surface diagram for ammonia synthesis on FCC Co(110) and HCP Co(10$\bar{1}$2) surfaces. The elementary reaction barriers and NH_3 desorption energy are indicated in eV.

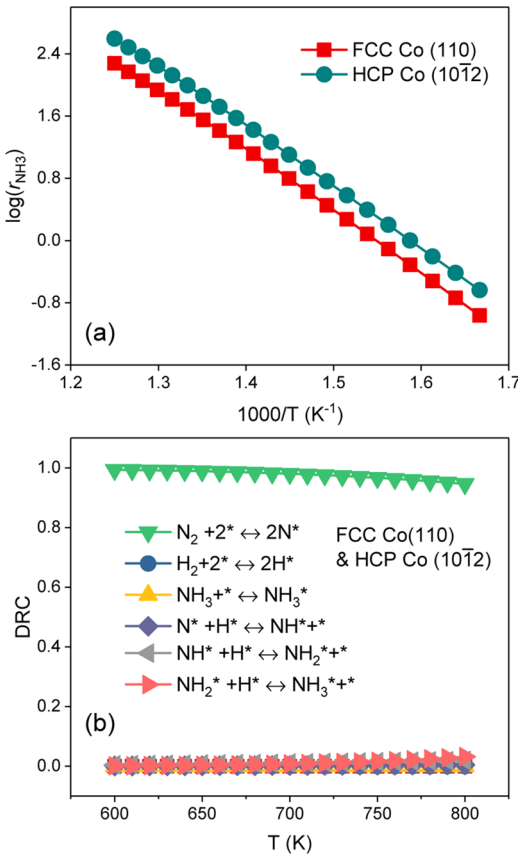

Figure 8. Calculated ammonia synthesis reaction rate (a) and degree of rate control analysis (b) on FCC Co(110) and HCP Co(10$\bar{1}$2) surfaces by full microkinetics simulations.

has higher activity than FCC Co for CO activation, even considering direct and H-assisted CO dissociation pathways.[54] There are at least four facets, namely, (11$\bar{2}$1), (10$\bar{1}$1), (10$\bar{1}$2), and (11$\bar{2}$0) on HCP Co, having direct CO dissociation rates higher than that of the most active FCC (100) facet by a factor of 10^5, 10^4, 10^2, and 2, respectively. Similar to CO activation, HCP Co is also more active than FCC Co for N_2 activation. However, the N_2 dissociation rate constants for the most active HCP (10$\bar{1}$2), (11$\bar{2}$1), and (10$\bar{1}$1) surfaces are only 4.7, 4.4, and 1.3 times higher than that of the most active FCC (110) surface, respectively. It indicates that CO activation is more sensitive to the surface structure and crystal structure of Co as compared with N_2 dissociation.

CO adsorbs strongly on Co metals. The calculated average adsorption energy of CO over HCP Co surfaces is −1.78 ± 0.088 eV, whereas it becomes −1.66 ± 0.058 eV for FCC Co. The difference of CO average adsorption energies between HCP Co and FCC Co is quite small (0.08 eV), suggesting a weak crystal sensitivity for the CO adsorption process. N_2 adsorption has the same behavior, i.e., the average adsorption energies are −0.54 ± 0.084 and −0.58 ± 0.074 eV for HCP and FCC Co, respectively. In analogy to CO adsorption, N_2 adsorption is also less structure sensitive regardless of FCC and HCP Co crystal structures. Different from CO, N_2 is much weakly bound to the Co surfaces, a fact of that affects effectively its approach to the surface and residence time on the surface, limiting its overall sticking probability of subsequent dissociative adsorption.

The dependence on surface structure and crystal structure is much more pronounced for CO and N_2 dissociations. We found that CO dissociation barriers are higher than those of N_2. The variation of CO dissociation barriers between the most active HCP Co and FCC Co surfaces is 0.53 eV, which is 0.43 eV larger than those of the N_2 dissociative adsorption reaction. To clarify the origin of the different behavior for N_2 and CO dissociation on HCP Co and FCC Co, we have investigated the adsorption energies of CO, N_2, C, N, and O atoms. In general, the stronger adsorption of CO compared with N_2 on Co surfaces can be interpreted from greater back donation with CO adsorption. The weak sensitivity toward the crystal structure for the adsorption of reactants (CO or N_2) cannot therefore rationalize the different activity for CO or N_2 dissociation between FCC and HCP Co.

Atomic C, N, and O adsorptions on Co surfaces are quite sensitive to the structure. Specifically, the C atom binding energies calculated with respect to isolated C atoms in the gas phase change from −6.83 to −8.15 for HCP Co and −6.80 to −8.01 eV for FCC Co surfaces. The variation of C atom binding energies is 1.32 eV for HCP Co and 1.21 eV for FCC Co distinct surfaces.[54] The substantial change of C atom binding energies between different surfaces originates from the C atom preferring to adsorb at the special 4-fold site of HCP Co and FCC Co surfaces. As stated above, the N atom binding energies vary from −5.56 to −6.39 eV for HCP Co and from −5.52 to −6.27 eV for FCC Co various surfaces. The variation of atomic N binding energies is 0.83 eV for HCP Co and 0.75 eV for FCC Co surfaces. The O atom binding energies are in the region of −5.63 to −6.06 eV for HCP Co and −5.50 to −5.99 eV for FCC Co. Thus, the binding energies of O atoms vary less than 0.43 eV for HCP Co and 0.49 eV for FCC Co surfaces. We found a general trend that C adsorbs much stronger than N and O atoms. N and O atoms have quite similar binding energies at the same site of HCP Co and FCC Co surfaces. Thus, the more stable adsorption of C atoms makes CO activation barriers significantly lower than that of N_2 activation. The distinct adsorption behavior between C, O, and N atoms can be ascribed to the different number of electrons present. C atom has four valence electrons and can form four strong chemical bonds. The stronger binding

DOI: 10.1021/acs.jpcc.9b00590
J. Phys. Chem. C 2019, 123, 10956−10966

strength of C atom compared to N and O atoms results in C atom adsorption being structurally more sensitive.

The CO and N_2 activation barriers are not only correlated with the binding strength of adsorbed atomic species but also the site competition between them. It is found that all CO or N_2 activation TSs have similar geometries on the same HCP Co and FCC Co surfaces, except for HCP $(10\bar{1}2)$ and FCC (311) and (110) surfaces. This can be ascribed to multiple effects including bond competition, adsorption of fragments, and bond length between the species at TSs. To clarify the origin for the different behavior of N_2 and CO activation, we take the two most active and representative HCP $(10\bar{1}1)$ and FCC (110) surfaces as an example. It is found that N_2 dissociative adsorption has a similar TS geometry compared to CO activation on HCP $(10\bar{1}1)$, whereas N_2 and CO activations have distinct TSs geometries on the FCC (110) surface, as seen in Figure 9.

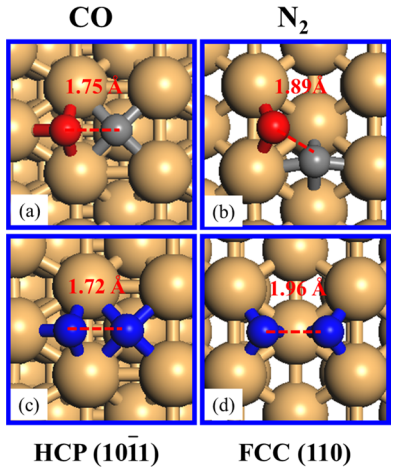

Figure 9. Top view of CO and N_2 dissociation transition state geometries on HCP Co$(10\bar{1}1)$ (a and c) and FCC Co(110) (b and d) surfaces. The gray and red spheres are C and O atoms, respectively.

The difference of CO activation barriers between the most active HCP Co$(10\bar{1}1)$ and FCC Co(110) surfaces is 0.49 eV, which is larger than that of N_2 activation by 0.40 eV. C atoms prefer to coordinate with four Co atoms on HCP Co$(10\bar{1}1)$ and FCC Co(110) surfaces with the binding energies of −8.03 and −7.08 eV at TSs, respectively. Furthermore, O atoms locate at the 3-fold sites and bridge sites at the TSs with the binding energies of −5.37 and −5.20 eV on HCP Co$(10\bar{1}1)$ and FCC Co(110) surfaces, respectively. The difference of C atom binding energies at TSs between HCP Co$(10\bar{1}1)$ and FCC Co(110) surfaces is −0.95 and −0.17 eV for O atoms, respectively. The repulsive interaction energy between C and O atoms at the TS on HCP Co$(10\bar{1}1)$ is 1.24 eV but 0.61 eV for the FCC Co(110) surface. The stronger adsorption of C atoms at the 4-fold site and O atoms at the 3-fold site, even with larger repulsive interactions between them, result in the HCP Co$(10\bar{1}1)$ surface having a much lower CO activation barrier compared to that of the FCC Co(110) surface. However, for N_2 dissociation on the HCP Co$(10\bar{1}1)$ surface, the binding energies of the two N atoms are −6.17 eV (4-fold site) and −5.22 eV (3-fold site) at the TS, whereas the binding energies of the two N atoms (3-fold site) become −5.08 eV at TS on the FCC Co(110) surface. The difference of two N atom binding energies between HCP Co$(10\bar{1}1)$ and FCC Co(110) surfaces is −1.09 eV but −0.14 eV for the other two N atoms. Meanwhile, the repulsive interaction energies are 1.56 and 0.41 eV between the two N atoms at TSs of HCP Co$(10\bar{1}1)$ and FCC Co(110) surfaces, respectively. Although the variation of atomic N binding energy is slightly larger compared with C adsorption at TSs between HCP Co$(10\bar{1}1)$ and FCC Co(110) surfaces, the even greater difference of the repulsive interaction energies between the two N atoms at TSs on HCP Co$(10\bar{1}1)$ and FCC Co(110) surfaces result in these two surfaces having a small difference in the activation barriers for N_2 activation. In conclusion, as compared to CO activation, the different N_2 activation TSs geometries on the FCC Co(110) surface makes N_2 dissociation less sensitive.

It is worth noting that HCP Co is more active than FCC Co for CO[54] and N_2 activation. However, for Ni and Ru,[45,49] the FCC structure is more active than the HCP structure for CO activation. It indicates that the crystal structure sensitivity is not only dependent on the composition of the transition metal but also the molecules adsorbed. Our work provides more insight into the crystal structure sensitivity for N_2 and CO activation.

4. CONCLUSIONS

In summary, the crystal structure sensitivity of nitrogen molecule dissociation and ammonia synthesis on Co was studied. DFT calculations show that irrespective of cobalt crystal phases, the interaction of cobalt catalysts with both nitrogen molecules and nitrogen atoms is weak. Dissociative adsorption energies and the corresponding dissociation barriers of nitrogen molecules are more structurally sensitive than the nitrogen molecular adsorption energy. First-principle microkinetic simulations show that nitrogen molecule dissociation and ammonia synthesis are sensitive to the surfaces exposed and crystal structures of Co catalysts. For nitrogen molecule dissociation, HCP Co is more active than FCC Co due to the higher intrinsic activity and higher density of active sites on HCP Co. Nitrogen molecule dissociation is the rate-determining step of ammonia synthesis on cobalt catalysts. Compared to CO activation, the influence of Co crystal structure on N_2 activation is weakened due to different transition states formed on FCC Co. The insights revealed from the present work are valuable for a mechanistic understanding of the crystal phase sensitivity on the activation of nitrogen molecules on cobalt, which could be used as a rational design for more efficient catalysts for ammonia synthesis.

■ ASSOCIATED CONTENT

Supporting Information

The Supporting Information is available free of charge on the ACS Publications website at DOI: 10.1021/acs.jpcc.9b00590.

Details of microkinetic modeling; convergence tests and calculated vibration frequency, partition functions, Gibbs free energy, equilibrium constant, and absolute ammonia synthesis reaction rate (PDF)

■ AUTHOR INFORMATION

Corresponding Authors

*E-mail: jinxun@umich.edu (J.-X.L.).
*E-mail: wxli70@ustc.edu.cn (W.-X.L.).

ORCID

Jin-Xun Liu: 0000-0002-7499-4197

DOI: 10.1021/acs.jpcc.9b00590
J. Phys. Chem. C 2019, 123, 10956−10966

Hai-Yan Su: 0000-0001-9326-9647
Wei-Xue Li: 0000-0002-5043-3088

Author Contributions

#B.-Y.Z. and P.-P.C. contributed equally to this work.

Notes

The authors declare no competing financial interest.

■ ACKNOWLEDGMENTS

We acknowledge funding from the National Key R&D Program of China (2017YFB0602205 and 2018YFA0208603), the Natural Science Foundation of China (91645202 and 21872136), and the Chinese Academy of Sciences (QYZDJ-SSW-SLH054).

■ REFERENCES

(1) Kojima, R.; Enomoto, H.; Muhler, M.; Aika, K.-i. Cesium-Promoted Rhenium Catalysts Supported on Alumina for Ammonia Synthesis. *Appl. Catal., A* **2003**, *246*, 311−322.
(2) Spencer, N.; Schoonmaker, R.; Somorjai, G. Iron Single Crystals as Ammonia Synthesis Catalysts: Effect of Surface Structure on Catalyst Activity. *J. Catal.* **1982**, *74*, 129−135.
(3) Ertl, G.; Knözinger, H.; Weitkamp, J. *Handbook of Heterogeneous Catalysis*; Wiley-VCH: Weinheim, 2008; Vol. *6*, pp 2965−2994.
(4) Brown, D. E.; Edmonds, T.; Joyner, R. W.; McCarroll, J. J.; Tennison, S. R. The Genesis and Development of the Commercial Bp Doubly Promoted Catalyst for Ammonia Synthesis. *Catal. Lett.* **2014**, *144*, 545−552.
(5) Hayashi, F.; Kitano, M.; Yokoyama, T.; Hara, M.; Hosono, H. Surface Treatment for Conductive 12cao Center Dot 7al(2)O(3) Electride Powder by Rapid Thermal Annealing Processing and Its Application to Ammonia Synthesis. *ChemCatChem* **2014**, *6*, 1317−1323.
(6) Chorkendorff, I.; Niemantsverdriet, J. W. *Concepts of Modern Catalysis and Kinetics*; John Wiley & Sons, 2017.
(7) Jacobsen, C. J. H.; Dahl, S.; Hansen, P. L.; Törnqvist, E.; Jensen, L.; Topsøe, H.; Prip, D. V.; Møenshaug, P. B.; Chorkendorff, I. Structure Sensitivity of Supported Ruthenium Catalysts for Ammonia Synthesis. *J. Mol. Catal. A: Chem.* **2000**, *163*, 19−26.
(8) Kojima, R.; Aika, K.-i. Rhenium Containing Binary Catalysts for Ammonia Synthesis. *Appl. Catal., A* **2001**, *209*, 317−325.
(9) Logadottir, A.; Rod, T. H.; Norskov, J. K.; Hammer, B.; Dahl, S.; Jacobsen, C. J. H. The Bronsted-Evans-Polanyi Relation and the Volcano Plot for Ammonia Synthesis over Transition Metal Catalysts. *J. Catal.* **2001**, *197*, 229−231.
(10) Hagen, S.; Barfod, R.; Fehrmann, R.; Jacobsen, C. J.; Teunissen, H. T.; Ståhl, K.; Chorkendorff, I. New Efficient Catalyst for Ammonia Synthesis: Barium-Promoted Cobalt on Carbon. *Chem. Commun.* **2002**, 1206−1207.
(11) Hagen, S.; Barfod, R.; Fehrmann, R.; Jacobsen, C. J.; Teunissen, H. T.; Chorkendorff, I. Ammonia Synthesis with Barium-Promoted Iron−Cobalt Alloys Supported on Carbon. *J. Catal.* **2003**, *214*, 327−335.
(12) Logadóttir, A.; Norskov, J. K. Ammonia Synthesis over a Ru(0001) Surface Studied by Density Functional Calculations. *J. Catal.* **2003**, *220*, 273−279.
(13) Hellman, A.; et al. Predicting Catalysis: Understanding Ammonia Synthesis from First-Principles Calculations. *J. Phys. Chem. B* **2006**, *110*, 17719−17735.
(14) Hellman, A.; Honkala, K.; Remediakis, I.; Logadottir, A.; Carlsson, A.; Dahl, S.; Christensen, C. H.; Nørskov, J. K. Ammonia Synthesis and Decomposition on a Ru-Based Catalyst Modeled by First-Principles. *Surf. Sci.* **2009**, *603*, 1731−1739.
(15) Luo, X.; Wang, R.; Ni, J.; Lin, J.; Lin, B.; Xu, X.; Wei, K. Effect of La_2o_3 on Ru/Ceo_2-La_2o_3 Catalyst for Ammonia Synthesis. *Catal. Lett.* **2009**, *133*, 382−387.
(16) Lendzion-Bieluń, Z.; Pelka, R.; Arabczyk, W. Study of the Kinetics of Ammonia Synthesis and Decomposition on Iron and Cobalt Catalysts. *Catal. Lett.* **2009**, *129*, 119−123.
(17) Hansgen, D. A.; Vlachos, D. G.; Chen, J. G. Using First Principles to Predict Bimetallic Catalysts for the Ammonia Decomposition Reaction. *Nat. Chem.* **2010**, *2*, 484−489.
(18) Wang, X.; Ni, J.; Lin, B.; Wang, R.; Lin, J.; Wei, K. Highly Efficient $Ru/Mgo−Ceo_2$ Catalyst for Ammonia Synthesis. *Catal. Commun.* **2010**, *12*, 251−254.
(19) Lin, B.; Wei, K.; Lin, J.; Ni, J. Effect of Treatment Conditions on Ruthenium Particle Size and Ammonia Synthesis Activity of Ruthenium Catalyst. *Catal. Commun.* **2013**, *39*, 14−19.
(20) Kitano, M.; Kanbara, S.; Inoue, Y.; Kuganathan, N.; Sushko, P. V.; Yokoyama, T.; Hara, M.; Hosono, H. Electride Support Boosts Nitrogen Dissociation over Ruthenium Catalyst and Shifts the Bottleneck in Ammonia Synthesis. *Nat. Commun.* **2015**, *6*, No. 6731.
(21) Lin, B.; Liu, Y.; Heng, L.; Ni, J.; Lin, J.; Jiang, L. Effect of Ceria Morphology on the Catalytic Activity of Co/Ceo2 Catalyst for Ammonia Synthesis. *Catal. Commun.* **2017**, *101*, 15−19.
(22) Gao, W.; Wang, P.; Guo, J.; Chang, F.; He, T.; Wang, Q.; Wu, G.; Chen, P. Barium Hydride-Mediated Nitrogen Transfer and Hydrogenation for Ammonia Synthesis: A Case Study of Cobalt. *ACS Catal.* **2017**, *7*, 3654−3661.
(23) Foster, S. L.; Bakovic, S. I. P.; Duda, R. D.; Maheshwari, S.; Milton, R. D.; Minteer, S. D.; Janik, M. J.; Renner, J. N.; Greenlee, L. F. Catalysts for Nitrogen Reduction to Ammonia. *Nat. Catal.* **2018**, *1*, 490−500.
(24) Jacobsen, C. J. H.; Dahl, S.; Clausen, B. S.; Bahn, S.; Logadottir, A.; Norskov, J. K. Catalyst Design by Interpolation in the Periodic Table: Bimetallic Ammonia Synthesis Catalysts. *J. Am. Chem. Soc.* **2001**, *123*, 8404−8405.
(25) Raróg-Pilecka, W.; Jedynak-Koczuk, A.; Petryk, J.; Miśkiewicz, E.; Jodzis, S.; Kaszkur, Z.; Kowalczyk, Z. Carbon-Supported Cobalt−Iron Catalysts for Ammonia Synthesis. *Appl. Catal., A* **2006**, *300*, 181−185.
(26) Kojima, R.; Aika, K.-i. Cobalt Molybdenum Bimetallic Nitride Catalysts for Ammonia Synthesis: Part 2. Kinetic Study. *Appl. Catal., A* **2001**, *218*, 121−128.
(27) Boisen, A.; Dahl, S.; Nørskov, J. K.; Christensen, C. H. Why the Optimal Ammonia Synthesis Catalyst Is Not the Optimal Ammonia Decomposition Catalyst. *J. Catal.* **2005**, *230*, 309−312.
(28) Zaera, F. The Surface Chemistry of Catalysis: New Challenges Ahead. *Surf. Sci.* **2002**, *500*, 947−965.
(29) Choudary, B. M.; Mulukutla, R. S.; Klabunde, K. J. Benzylation of Aromatic Compounds with Different Crystallites of Mgo. *J. Am. Chem. Soc.* **2003**, *125*, 2020−2021.
(30) Honkala, K.; Hellman, A.; Remediakis, I. N.; Logadottir, A.; Carlsson, A.; Dahl, S.; Christensen, C. H.; Norskov, J. K. Ammonia Synthesis from First-Principles Calculations. *Science* **2005**, *307*, 555−558.
(31) Ducreux, O.; Lynch, J.; Rebours, B.; Roy, M.; Chaumette, P. In Situ Characterisation of Cobalt Based Fischer-Tropsch Catalysts: A New Approach to the Active Phase. *Stud. Surf. Sci. Catal.* **1998**, *119*, 125−130.
(32) Park, J.-N.; Noh, J.; Chang, J.-S.; Park, S.-E. Ethylbenzene to Styrene in the Presence of Carbon Dioxide over Zirconia. *Catal. Lett.* **2000**, *65*, 75−78.
(33) Enache, D. I.; Rebours, B.; Roy-Auberger, M.; Revel, R. In Situ Xrd Study of the Influence of Thermal Treatment on the Characteristics and the Catalytic Properties of Cobalt-Based Fischer−Tropsch Catalysts. *J. Catal.* **2002**, *205*, 346−353.
(34) De la Peña O'Shea, V. A.; Homs, N.; Fierro, J. L. G.; Ramírez de la Piscina, P. Structural Changes and Activation Treatment in a Co/Sio_2 Catalyst for Fischer−Tropsch Synthesis. *Catal. Today* **2006**, *114*, 422−427.
(35) Ducreux, O.; Rebours, B.; Lynch, J.; Roy-Auberger, M.; Bazin, D. Microstructure of Supported Cobalt Fischer-Tropsch Catalysts. *Oil Gas Sci. Technol.* **2008**, *64*, 49−62.

DOI: 10.1021/acs.jpcc.9b00590
J. Phys. Chem. C 2019, 123, 10956−10966

(36) de la Peña O' Shea, V. A.; de la Piscina, P. R.; Homs, N.; Aromí, G.; Fierro, J. L. G. Development of Hexagonal Closed-Packed Cobalt Nanoparticles Stable at High Temperature. *Chem. Mater.* **2009**, *21*, 5637−5643.
(37) Khodakov, A. Y. Fischer-Tropsch Synthesis: Relations between Structure of Cobalt Catalysts and Their Catalytic Performance. *Catal. Today* **2009**, *144*, 251−257.
(38) Wu, G.; Tan, X.; Li, G.; Hu, C. Effect of Preparation Method on the Physical and Catalytic Property of Nanocrystalline Fe_2o_3. *J. Alloys Compd.* **2010**, *504*, 371−376.
(39) Karaca, H.; Safonova, O. V.; Chambrey, S.; Fongarland, P.; Roussel, P.; Griboval-Constant, A.; Lacroix, M.; Khodakov, A. Y. Structure and Catalytic Performance of Pt-Promoted Alumina-Supported Cobalt Catalysts under Realistic Conditions of Fischer−Tropsch Synthesis. *J. Catal.* **2011**, *277*, 14−26.
(40) Sadeqzadeh, M.; Karaca, H.; Safonova, O.; Fongarland, P.; Chambrey, S.; Roussel, P.; Griboval-Constant, A.; Lacroix, M.; Curulla-Ferré, D.; Luck, F.; et al. Identification of the Active Species in the Working Alumina-Supported Cobalt Catalyst under Various Conditions of Fischer−Tropsch Synthesis. *Catal. Today* **2011**, *164*, 62−67.
(41) Mou, X.; Zhang, B.; Li, Y.; Yao, L.; Wei, X.; Su, D. S.; Shen, W. Rod-Shaped Fe_2o_3 as an Efficient Catalyst for the Selective Reduction of Nitrogen Oxide by Ammonia. *Angew. Chem., Int. Ed.* **2012**, *51*, 2989−2993.
(42) Kusada, K.; Kobayashi, H.; Yamamoto, T.; Matsumura, S.; Sumi, N.; Sato, K.; Nagaoka, K.; Kubota, Y.; Kitagawa, H. Discovery of Face-Centered-Cubic Ruthenium Nanoparticles: Facile Size-Controlled Synthesis Using the Chemical Reduction Method. *J. Am. Chem. Soc.* **2013**, *135*, 5493−5496.
(43) Gnanamani, M. K.; Jacobs, G.; Shafer, W. D.; Davis, B. H. Fischer−Tropsch Synthesis: Activity of Metallic Phases of Cobalt Supported on Silica. *Catal. Today* **2013**, *215*, 13−17.
(44) Prieto, G.; Concepción, P.; Murciano, R.; Martínez, A. The Impact of Pre-Reduction Thermal History on the Metal Surface Topology and Site-Catalytic Activity of Co/Sio2 Fischer−Tropsch Catalysts. *J. Catal.* **2013**, *302*, 37−48.
(45) Liu, J.-X.; Zhang, B.-Y.; Chen, P.-P.; Su, H.-Y.; Li, W.-X. Co Dissociation on Face-Centered Cubic and Hexagonal Close-Packed Nickel Catalysts: A First-Principles Study. *J. Phys. Chem. C* **2016**, *120*, 24895−24903.
(46) Ye, H.; Wang, Q.; Catalano, M.; Lu, N.; Vermeylen, J.; Kim, M. J.; Liu, Y.; Sun, Y.; Xia, X. Ru Nanoframes with an Fcc Structure and Enhanced Catalytic Properties. *Nano Lett.* **2016**, *16*, 2812−2817.
(47) AlYami, N. M.; LaGrow, A. P.; Joya, K. S.; Hwang, J.; Katsiev, K.; Anjum, D. H.; Losovyj, Y.; Sinatra, L.; Kim, J. Y.; Bakr, O. M. Tailoring Ruthenium Exposure to Enhance the Performance of Fcc Platinum@ Ruthenium Core−Shell Electrocatalysts in the Oxygen Evolution Reaction. *Phys. Chem. Chem. Phys.* **2016**, *18*, 16169−16178.
(48) Yao, Y.; He, D. S.; Lin, Y.; Feng, X.; Wang, X.; Yin, P.; Hong, X.; Zhou, G.; Wu, Y.; Li, Y. Modulating Fcc and Hcp Ruthenium on the Surface of Palladium−Copper Alloy through Tunable Lattice Mismatch. *Angew. Chem., Int. Ed.* **2016**, *55*, 5501−5505.
(49) Li, W.-Z.; et al. Chemical Insights into the Design and Development of Face-Centered Cubic Ruthenium Catalysts for Fischer−Tropsch Synthesis. *J. Am. Chem. Soc.* **2017**, *139*, 2267−2276.
(50) Liu, J. X.; Li, W. X. Theoretical study of crystal phase effect in heterogeneous catalysis. *Wiley Interdiscip. Rev.: Comput. Mol. Sci.* **2016**, *6*, 571−583.
(51) Liu, J.-X.; Wang, P.; Xu, W.; Hensen, E. J. M. Particle Size and Crystal Phase Effects in Fischer-Tropsch Catalysts. *Engineering* **2017**, *3*, 467−476.
(52) Kitakami, O.; Sato, H.; Shimada, Y.; Sato, F.; Tanaka, M. Size Effect on the Crystal Phase of Cobalt Fine Particles. *Phys. Rev. B* **1997**, *56*, No. 13849.
(53) Fischer, N.; van Steen, E.; Claeys, M. Preparation of Supported Nano-Sized Cobalt Oxide and Fcc Cobalt Crystallites. *Catal. Today* **2011**, *171*, 174−179.
(54) Liu, J.-X.; Su, H.-Y.; Sun, D.-P.; Zhang, B.-Y.; Li, W.-X. Crystallographic Dependence of Co Activation on Cobalt Catalysts: Hcp Versus Fcc. *J. Am. Chem. Soc.* **2013**, *135*, 16284−16287.
(55) Liu, J.-X.; Su, H.-Y.; Li, W.-X. Structure Sensitivity of Co Methanation on Co(0001), and Surfaces: Density Functional Theory Calculations. *Catal. Today* **2013**, *215*, 36−42.
(56) Shetty, S.; Jansen, A. P. J.; van Santen, R. A. Direct Versus Hydrogen-Assisted Co Dissociation. *J. Am. Chem. Soc.* **2009**, *131*, 12874−12875.
(57) Petersen, M. A.; van den Berg, J.-A.; Ciobîcă, I. M.; van Helden, P. Revisiting Co Activation on Co Catalysts: Impact of Step and Kink Sites from Dft. *ACS Catal.* **2017**, *7*, 1984−1992.
(58) Harmel, J.; Peres, L.; Estrader, M.; Berliet, A.; Maury, S.; Fécant, A.; Chaudret, B.; Serp, P.; Soulantica, K. Hcp-Co Nanowires Grown on Metallic Foams as Catalysts for Fischer−Tropsch Synthesis. *Angew. Chem.* **2018**, *57*, 10579−10583.
(59) Lyu, S.; et al. Role of Active Phase in Fischer−Tropsch Synthesis: Experimental Evidence of Co Activation over Single-Phase Cobalt Catalysts. *ACS Catal.* **2018**, *8*, 7787−7798.
(60) Kresse, G.; Furthmüller, J. Efficient Iterative Schemes for Ab Initio Total-Energy Calculations Using a Plane-Wave Basis Set. *Phys. Rev. B* **1996**, *54*, No. 11169.
(61) Kresse, G.; Hafner, J. Ab Initio Molecular Dynamics for Liquid Metals. *Phys. Rev. B* **1993**, *47*, No. 558.
(62) Kresse, G.; Joubert, D. From Ultrasoft Pseudopotentials to the Projector Augmented-Wave Method. *Phys. Rev. B* **1999**, *59*, No. 1758.
(63) Perdew, J. P.; Burke, K.; Ernzerhof, M. Generalized Gradient Approximation Made Simple. *Phys. Rev. Lett.* **1996**, *77*, 3865−3868.
(64) Monkhorst, H. J.; Pack, J. D. Special Points for Brillouin-Zone Integrations. *Phys. Rev. B* **1976**, *13*, 5188−5192.
(65) Vincent, F.; Figlarz, M. C. R. H. *Seances Acad. Sci.* **1967**, *264*, No. 1270.
(66) Sun, K.; Zhao, Y.; Su, H. Y.; Li, W. X. Force Reversed Method for Locating Transition States. *Theor. Chem. Acc.* **2012**, *131*, 1−10.
(67) Henkelman, G.; Uberuaga, B. P.; Jónsson, H. A Climbing Image Nudged Elastic Band Method for Finding Saddle Points and Minimum Energy Paths. *J. Chem. Phys.* **2000**, *113*, 9901−9904.
(68) Turmanova, S.; Genieva, S.; Vlaev, L. Kinetics of Non-isothermal Degradation of Some Polymer Composites: Change of Entropy at the Formation of the Activated Complex from the Reagents. *J. Thermodyn.* **2011**, *2011*, No. 605712.
(69) Wulff, G. On the Question of Speed of Growth and Dissolution of Crystal Surfaces. *Z. Kristallogr.* **1901**, *34*, 449−530.
(70) Hansen, P. L.; Wagner, J. B.; Helveg, S.; Rostrup-Nielsen, J. R.; Clausen, B. S.; Topsøe, H. J. S. Atom-resolved imaging of dynamic shape changes in supported copper nanocrystals. *Science* **2002**, *295*, 2053−2055.
(71) Gonzalez-DelaCruz, V. M.; Holgado, J. P.; Pereñíguez, R.; Caballero, A. Morphology changes induced by strong metal−support interaction on a Ni−ceria catalytic system. *J. Catal.* **2008**, *257*, 307−314.
(72) Uchiyama, T.; Yoshida, H.; Kuwauchi, Y.; Ichikawa, S.; Shimada, S.; Haruta, M.; Takeda, S. J. A. C. I. E. Systematic morphology changes of gold nanoparticles supported on CeO2 during CO oxidation. *Angew. Chem., Int. Ed.* **2011**, *50*, 10157−10160.
(73) Liu, J.-X.; Su, Y.; Filot, I. A. W.; Hensen, E. J. M. A Linear Scaling Relation for Co Oxidation on Ceo2-Supported Pd. *J. Am. Chem. Soc.* **2018**, *140*, 4580−4587.
(74) Blyholder, G. Molecular Orbital View of Chemisorbed Carbon Monoxide. *J. Phys. Chem.* **1964**, *68*, 2772−2777.
(75) Blyholder, G. Cndo Model of Carbon Monoxide Chemisorbed on Nickel. *J. Phys. Chem.* **1975**, *79*, 756−761.
(76) Kang, D. B. A Comparative Study of the Bonding of N2 and Co to Ru (001) and the Role of 5σ Orbital in Their Molecular Vibrational Frequency Changes. *Bull. Korean Chem. Soc.* **1999**, *20*, 247−249.
(77) Liu, Z.-P.; Hu, P.; Lee, M.-H. Insight into Association Reactions on Metal Surfaces: Density-Functional Theory Studies of

DOI: 10.1021/acs.jpcc.9b00590
J. Phys. Chem. C 2019, 123, 10956−10966

Hydrogenation Reactions on Rh (111). *J. Chem. Phys.* **2003**, *119*, 6282−6289.
(78) Bligaard, T.; Nørskov, J. K.; Dahl, S.; Matthiesen, J.; Christensen, C. H.; Sehested, J. The Brønsted−Evans−Polanyi Relation and the Volcano Curve in Heterogeneous Catalysis. *J. Catal.* **2004**, *224*, 206−217.
(79) Masel, R. I. *Chemical Kinetics and Catalysis*; Wiley-Interscience: NY, 2001.
(80) Zhang, B.-Y.; Su, H.-Y.; Liu, J.-X.; Li, W.-X. Interplay between Site Activity and Density of Bcc Iron for Ammonia Synthesis Based on First-Principles Theory. *ChemCatChem* **2019**, *11*, 1928−1934.
(81) Filot, I. A. W.; van Santen, R. A.; Hensen, E. J. M. The Optimally Performing Fischer−Tropsch Catalyst. *Angew. Chem., Int. Ed.* **2014**, *126*, 12960−12964.
(82) Filot, I. A.; Broos, R. J.; van Rijn, J. P.; van Heugten, G. J.; van Santen, R. A.; Hensen, E. J. First-Principles-Based Microkinetics Simulations of Synthesis Gas Conversion on a Stepped Rhodium Surface. *ACS Catal.* **2015**, *5*, 5453−5467.
(83) http://www.mkmcxx.nl/.

DOI: 10.1021/acs.jpcc.9b00590
J. Phys. Chem. C 2019, 123, 10956−10966